A 4-MEGAVOLT, 5-KILOAMPERE PULSED-POWER HIGH-BRIGHTNESS ELECTRON BEAM SOURCE*

K. L. Carlson, L. A. Bollita, T. J. Kauppila, D. C. Moir, and K. N. Riglon
Los Alamos National Laboratory
P. O. Box 1663
Los Alamos, New Mexico 87545

T. P. Hughes
Mission Research Corporation
Albuquerque, New Mexico 87106-4245

Abstract

The REX machine at Los Alamos is being used to generate a 4-MV, 5-kA, 50-ns electron beam. The beam is produced by a planar velvet cathode, accelerated through a foilless anode aperture, and transported by an air core magnetic lens. Extensive measurements of the time-resolved (<1 ns) properties of the beam using a streak camera and high speed electronic diagnostics have been made. These parameters include beam current, voltage, current density, and emittance for a single cathode/anode configuration. Results indicate beam brightness in excess of $10^8 A/m^2-rad^2$. Numerical simulations of the experiment have been performed with ISIS, a time-dependent PIC code, and are in good agreement with the measurements. This electron beam source is being considered as an injector to a linear induction accelerator and can be operated at higher voltages and currents as a stand-alone flash x-ray machine.

1. Introduction

The Relativistic Electron-Beam Experiment (REX) machine at LANL is used to generate a 4-MV, 5-kA, 50-ns electron beam. The generation and transport of this beam is being carefully examined for its potential application as an injector for the Dual Axis Radiographic Hydro-Test Facility (DARHT) accelerators. Measurements of the time-resolved electron beam current, voltage, and emittance produced by a velvet cathode are presented in comparison with ISIS particle-in-cell simulations (Ref. 1). The experimental arrangement is discussed in Section 2 and the data and results are presented in Section 3.

2. Experimental Arrangement

The electron source consists of a 76.2-mm diam velvet cathode mounted on a field forming electrode (Fig. 1). The velvet cloth is inset in the surface of the cathode assembly about 1 mm to keep the fiber tips flush with the metal surface. The aluminum field forming electrode, which is coated with glyptal to suppress emission, is flat in the anode region. The anode/cathode (A-K) gap is 147.6 mm and the anode aperture is 152-mm diam. The field forming electrode is centered on a Lucite-radial insulator with embedded aluminum grading rings. The insulator assembly separates the oil-filled pulse forming line (PFL) from the vacuum diode and contains a 125-Ω radial-liquid resistor. The stainless steel vacuum vessel which includes the anode is cryogenically pumped. Typical vacuum in the A-K region is 3×10^{-5} torr.

The magnetic field used for beam extraction is generated by a 1.7-m-i.d. bucking coil centered 145 mm behind the cathode and a 244-mm-long, air-core, solenoid extraction magnet whose center is located 377.0 mm from the cathode. The inside and outside radii of the solenoid are 114 mm and 216 mm, respectively. Figure 2 is a map of the axial magnetic field as a function of axial position (z) and radius (r) about the axis of the machine. The voltage pulse produced by the Marx generator/PFL is routinely measured with capacitive (E-dot) monitors located in the oil-filled transmission line before the radial resistor and in a plane that is midway across the A-K gap on the vacuum side. The voltage monitors have been calibrated by measuring the electron beam energy with a magnetic spectrometer. The current is measured with four symmetrically located, magnetic sense (B-dot) loops. The current is measured before the radial resistor (I-tube), in the vacuum (I-total), at the anode aperture 211 mm from the cathode (I-diode), and at the drift tube 720 mm from the cathode (I-transport). The four symmetric signals from the B-dot loops are summed passively at the machine and transmitted along with the E-dot signals to a screen room using ~ 30 m of RG214. The pulse currents and voltages are integrated with 1-μs time constant 50-Ω integrators recorded on Tektronix 7103 oscilloscopes. The bandwidth of the measurements is limited by cable attenuation at the higher frequencies.

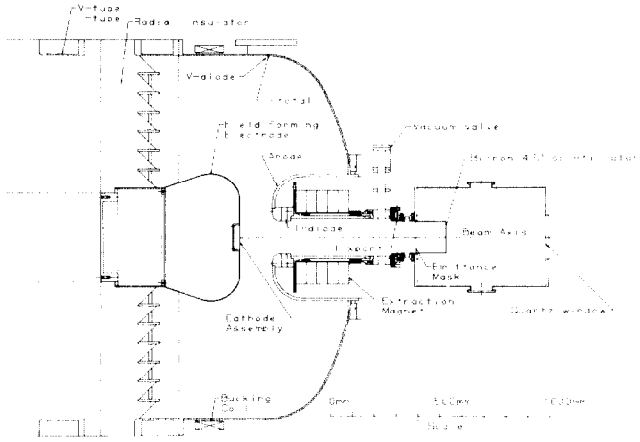

Fig. 1. REX Experimental Hardware.

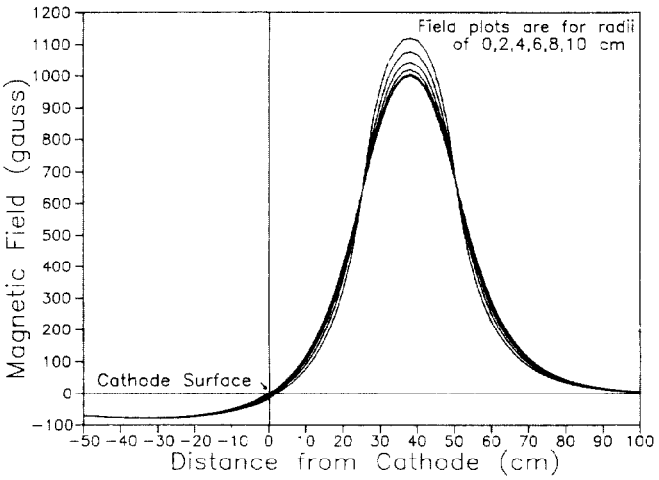

Fig. 2. Magnetic Field Map for Fig. 1.

The emittance of the electron beam is measured by

Work performed under the auspices of the U.S. Department of Energy.

CH2669-0/89/0000-0276$01.00©1989 IEEE

intercepting the beam with a brass disc (3.2-mm thick, 216-mm diam), which contains a linear array of 17, 1-mm diam holes separated by 10 mm, located vertically along the diameter. The mask is located 817 mm from the cathode. The measurement is made with the electron beam nearly collimated at a diameter of ~ 100 mm. The peak extraction magnet field to produce this beam condition is 850 G. The beam that is transmitted through the holes drifts 204 mm before striking a 0.5-mm-thick strip of Bicron 422 scintillator. Light from the scintillator is imaged onto the photocathode of an IMACON 500 streak camera using a 3.5-inch-diam Questar telescope and two turning mirrors. Typical sweep speed for all of the measurements was 2 ns/mm. Time resolution of the streak camera data was limited by the 1.3-ns FWHM response time of the scintillator. Streak data were recorded on Kodak Royal X-Pan (RXP) film.

3. Data and Results

Oscillograph traces of the voltage (V-tube) and current monitor (I-diode) are shown in Figs. 3a and 3b, respectively. As stated above, the voltage monitor was calibrated using a magnetic spectrometer. The resulting constant is 2.55 ± 0.04 MV/V. The current monitor was inserted in a 50-Ω coaxial pulse line described in Ref. 2 and yielded a calibration constant of 6.05 ± 0.30 kA/V.

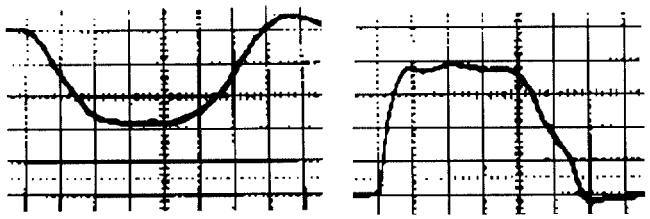

Fig. 3. V-tube and I-diode at 3.8 MV (0.5 V/div) and 4.8 kA (0.2 V/div) Recorded at 10 ns/div.

Figure 4 is a plot of electron beam current versus voltage. Experimental data, obtained by varying the Marx charge voltage, are shown as diamonds with the error bars indicating the current uncertainty. The upper curve with circles is the result of a simulation using the ISIS particle-in-cell code (Ref. 3). Middle and lower curves come from Child-Langmuir (Ref. 4) nonrelativistic planar diode and Jory-Trivelpiece (Ref. 5) relativistic planar diode, respectively. The experimentally measured current is almost twice that expected from a simple planar relativistic diode. Experimental data are in reasonable agreement with ISIS calculations, but are systematically lower.

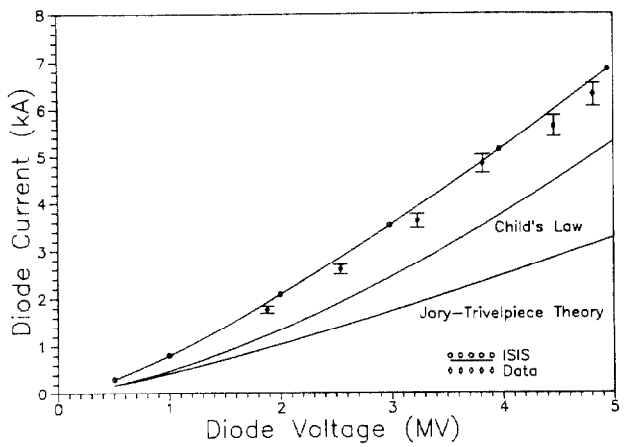

Fig. 4. Beam Current vs Voltage for 76.2-mm-diam Cathode and A-K Gap of 150 mm.

Photographic reproduction of a streak camera emittance measurement is shown in Fig. 5. Time sweep is from left to right and from the start to the end of light is 50 ns, in agreement with electrical measurements. The voltage across the A-K gap is relatively flat across 30 ns of the pulse. The streak record on RXP film is scanned with a 50-μm aperture using a microdensitometer. The subsequent film density is converted to relative light intensity by using the exposure curve obtained for the RXP film with local processing. The analysis is generally performed on the 30-ns flat top of the pulse, where the beam energy variation is ± 1.5%. The data are time averaged over the 30-ns flat top and additionally sampled at the center of the pulse over 1 ns. In either case, the analysis to obtain the emittance is the same. Figure 6 is a plot of relative beam intensity as a function of x obtained from the emittance mask streak record. Each of the distributions represents a sample of the beam that is transmitted through the 1-mm-diam hole in the mask. A beam that is cold (born with no transverse energy) would generate a rectangular distribution 1 mm in diameter. Because of finite temperature, the beams have gaussian distributions. The location of the peaks relative to the mask yields information on beam convergence as well as beam radius. These data are used to produce an x-x' plot, where 90% of the beam is included in the temperature as well as the diameter (Fig. 7).

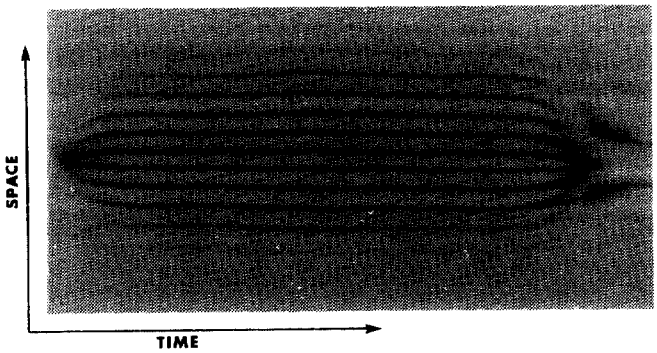

Fig. 5. Streak Record of Emittance Mask.

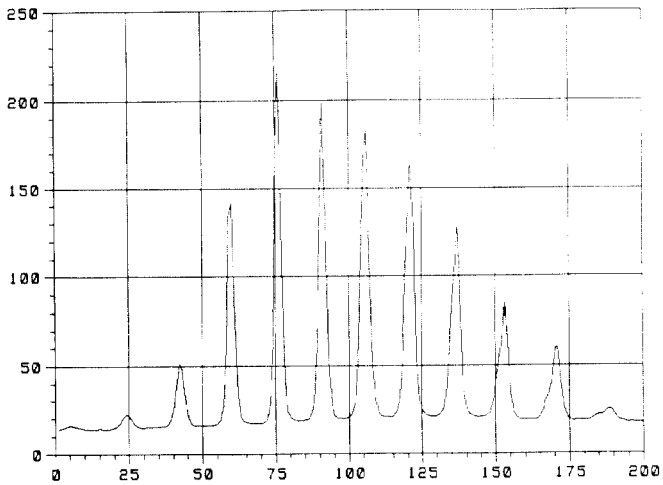

Fig. 6. Relative Intensity of Beamlets Across the Center of the Beam.

Overlayed on the x-x' plot are the x-x' results of cold beam simulations by Mission Research Corporation (Ref. 3) and LLNL (Ref. 6). The simulations include the effect of the emittance mask that shorts the radial electric field. Clearly, nonlinear space-charge affects the measurement, and these simulations included the mask in order to make comparisons with the experimental results. Figures 8a and 8b are ISIS simulations with the radial electric field shorted at

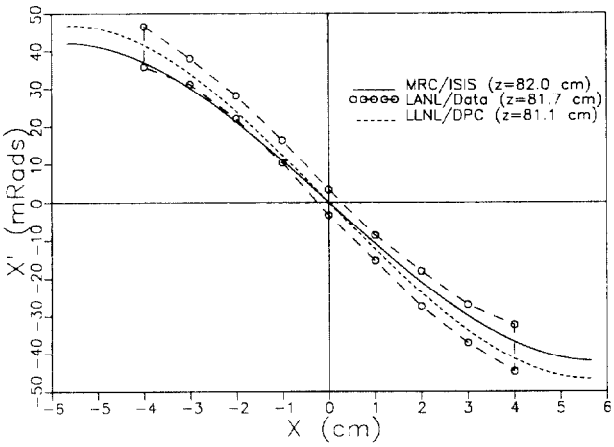

Fig. 7. REX Electron Beam Emittance Integrated over 30 ns at 3.8 MV and 4.8 kA.

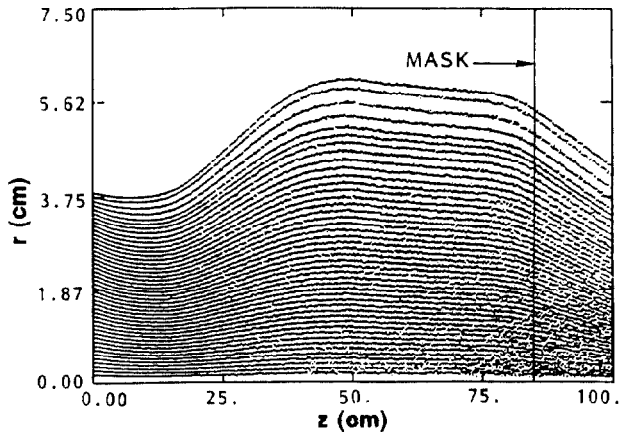

Fig. 8a. ISIS Simulation with Emittance Mask.

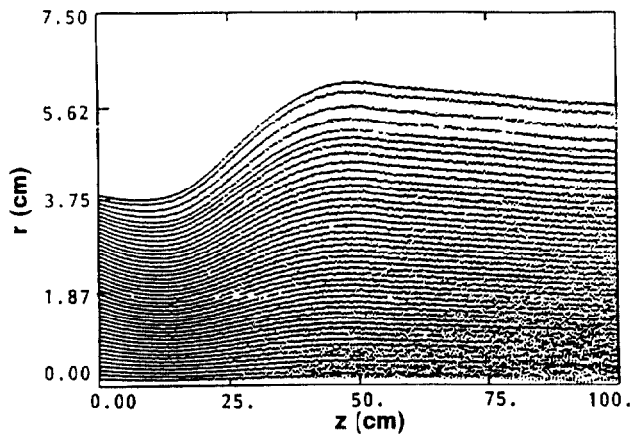

Fig. 8b. ISIS Simulation without Emittance Mask.

the emittance mask location and show the effect of no emittance mask. The edge emittance of the beam for Fig. 7 is obtained by calculating the phase space area of the x–x' plot divided by π, and gives values of 0.12 and 0.058 cm–rad for data integrated over 30 and 1 ns, respectively. The corresponding Lapostolle emittance from ISIS is 0.05 cm–rad for a monoenergetic beam, and therefore, must be compared to the 1–ns data. The brightness of the REX beam at 4 MV and 5 kA integrated over the 30 ns flat top is 3.5 x 10^8 A/m^2–rad^2.

The effective cathode temperature can be measured by examining a single beamlet coming from the center of the mask. The center beamlet produces a gaussian intensity distribution with an x_{rms} = 0.42 mm; the mask hole radius is 0.5 mm. This produces an effective temperature of 130 eV (Ref. 5). The temperature predicted according to Ref. 7 is 18 eV using a cathode radius of 38.1 mm; this discrepancy is not understood at present.

4. Conclusion

Extensive measurements of the time–resolved properties of the electron beam have been presented and compared with simulations. Agreement between simulation and experiment is excellent; therefore, ISIS can be used as a tool to design an electron injector for DARHT. This agreement is exemplified by the x–x' plot, where the only input to the code is the beam energy as measured by the spectrometer and the extraction magnet field $B_z(r,z)$. The remaining beam dynamics issues are completely predicted by the simulation. Therefore, the nonlinear space–charge forces, extracted current, beam transport, and focusing are correctly calculated by the code.

References

[1] ISIS was written by M. E. Jones at Los Alamos National Laboratory.

[2] R. L. Carlson, R. N. Ridlon, and L. E. Stout, RSI Vol. 57, No. 10, 2471 (1986).

[3] C. D. Child, Phys. Rev. 32, 492 (1913); I. Langmuir, Phys. Rev. 2, 450 (1913).

[4] H. R. Jory and A. W. Trivelpiece, JAP 40, 1180 (1977).

[5] T. P. Hughes, R. M. Clark, R. L. Carlson, L. A. Builta, T. J. Kauppila, D. C. Moir, and R. N. Ridlon, Report MRC/ABQ–R–1133, February 1989, pp. 9–18.

[6] DPC calculations were performed by John Boyd of Lawrence Livermore National Laboratory.

[7] Y. Y. Lau, JAP 61, 36 (1987).